Corrosion Science 206 (2022) 110477

Contents lists available at ScienceDirect

Corrosion Science

journal homepage: www.elsevier.com/locate/corsci

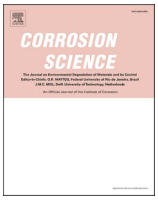

The kinetics and mechanism of filiform corrosion affecting organic coated Mg alloy surfaces

Christos Kousis [a,*], Patrick Keil [b], Hamilton, Neil McMurray [a], Geraint Williams [a]

[a] Materials Research Centre, College of Engineering, Swansea University Bay Campus, Crymlyn Burrows, Swansea SA1 8EN, UK
[b] BASF Coatings GmbH, Glasuritstrasse 1, 48165 Münster, Germany

ARTICLE INFO

Keywords:
Magnesium alloy
Organic coating
Anodic disbondment
Filiform corrosion

ABSTRACT

The filiform corrosion (FFC) of organic coated magnesium alloys is investigated using in-situ scanning Kelvin probe and time-lapse photography. FFC is initiated by injecting $MgCl_2$, HCl and $FeCl_2$ into a coating defect and ensuing FFC propagation rates are shown to increase as a logarithmic function of the chloride ion concentration and are strongly dependent on relative humidity. Post-corrosion surface analysis shows chloride abundance near the filament leading edge and evidence of sequestration within corroded regions behind. The FFC mechanism is consistent with chloride-induced anodic dissolution at the front coupling with water reduction on a cathodically-activated corroded surface behind.

1. Introduction

Recent years have seen an increased interest in the use of magnesium (Mg) and its alloys as structural metals, primarily because of their good strength-to-weight ratio and high specific strength [1]. Magnesium is 35% lighter than aluminium and 75% lighter than steel [2], making Mg and its alloys ideal candidates for automotive and aerospace applications where weight reduction is desirable. However, Mg and its alloys also require protection from environmental degradation since they are susceptible to corrosion due to their position in the electrochemical series. Although there are many published works which focus on surface treatments and inorganic conversion coatings as a means of improving corrosion resistance [3,4], relatively few publications are devoted to investigations of organic coatings for corrosion protection for Mg and its alloys [5,6]. Furthermore, the lack of understanding of the prevailing mechanisms of organic coating failure on magnesium and its alloys has hindered the adequate development of organic coating technologies which are tailored for magnesium alloys.

When organic coated magnesium substrates are exposed to an atmosphere comprising a high relative humidity (RH) and aggressive inorganic salts, coating failure can proceed according to two principal mechanisms: cathodic delamination [7] and/or filiform corrosion (FFC) [8–10]. Corrosion-driven failure typically initiates at penetrative coating defect such as cut-edges, scratches, and scribes where aggressive species, such as chloride ions can make contact to the bare metal and access the coating-substrate interface. Blistering is another phenomenon which can also occur especially at extremely high levels of relative humidity, normally through an intact organic coating [11–13]. In a previous study, employing model poly-vinyl butyral (PVB) coatings applied to automotive E717 Mg alloy surfaces under atmospheric corrosion conditions, we demonstrated that the mechanism of coating failure originating from a penetrative coating defect was highly dependent upon the nature of the chloride salt employed to initiate corrosion [7]. When underfilm corrosion was initiated using group I chloride salts, coating failure was characterised by the rapid development of a halo of disbonded coating surrounding the defect region, which expanded radially with time. Post corrosion surface analysis showed that the region affected by the halo was abundant in the initiating cation, but that chloride ions were not present and were conserved within the defect region. It was thus proposed that a cathodic disbondment mechanism was responsible for this phenomenon in which anodic magnesium dissolution at the defect is coupled with underfilm cathodic hydrogen evolution. However, in the absence of group I cations, which can sustain ionic current within a region of high alkalinity, no such disbondment halo was observed. Consequently, the use of HCl or $MgCl_2$ to initiate coating failure produced only anodic disbondment via filiform-like corrosion (FFC), characterised by the underfilm evolution of a network of dark tracks which lengthen with time.

FFC is well known to affect other organic coated metal surfaces, such as iron [14–17] and aluminium alloys [12,18–20], where the

* Corresponding author.
E-mail addresses: 922387@swansea.ac.uk, chrkousis@gmail.com (C. Kousis).

https://doi.org/10.1016/j.corsci.2022.110477
Received 14 February 2022; Received in revised form 3 July 2022; Accepted 5 July 2022
Available online 7 July 2022

propagation of filaments is considered to proceed through a differential aeration cell located at the electrolyte-filled head at the filament leading edge. An oxygen concentration cell results from facile transport of O_2 through the corrosion product filled tail to the rear of the filament head [21], with a local anode at the leading-edge producing undermining of the organic coating. However, it has been proposed in the case of PVB coated Mg, that where hydrogen evolution according to Eq. (1) is anticipated to be the dominant cathodic reaction, the mechanism of FFC propagation involves anodic Mg dissolution (Eq. (2)) coupling with cathodic water reduction on a cathodically activated, corroded surface immediately behind the filament leading edge. This differential electrocatalytic activation provides the driving force for filament advancement and explains in part why FFC rates of propagation remain unchanged in the absence of oxygen when PVB-coated Mg is maintained at a high relative humidity.

$$2H_2O + 2e^- \rightarrow H_2 + 2OH^- \quad (1)$$

$$Mg \rightarrow Mg^{2+} + 2e^- \quad (2)$$

In this work, the influence of factors such as chloride ion concentration and relative humidity on the kinetics of FFC propagation on model PVB-coated Mg alloy substrates, is systematically investigated using a combination of in-situ time-lapse photography and the Scanning Kelvin Probe (SKP). The investigation has concentrated on a technologically important, rare-earth containing E717 (Electron™ 717) alloy, also known as ZEK100 (ZE10 type alloy) which is considered as a promising candidate for automotive applications due to its favourable mechanical properties [22,23]. It should also be noted that several recent publications [7,24–28] are devoted to furthering the understanding of the corrosion behaviour of this particular alloy. In addition, some key experiments are also repeated using other widely used AZ-series Mg alloys, such as the AZ31 and AZ91 to confirm FFC susceptibility under the same conditions. The principal aims are (i): to confirm whether observations regarding chloride-induced FFC initiation and propagation in the absence of group I cations, previously reported for pure Mg [10] also hold true for commercially available alloys, and (ii) to identity the influence of chloride ion concentration, relative humidity and the absence of oxygen on underfilm corrosion rates. FFC is inoculated by applying controlled quantities of aqueous HCl, $MgCl_2$ or $FeCl_2$ to scribed defects in PVB coated alloy specimens and quantification of FFC kinetics is achieved by time-dependent analysis of corrosion-affected areas via time-lapse photography. $FeCl_2$ was selected to test out a hypothesis regarding the role of iron impurity redeposition in contributing to the cathodic activation of corroding Mg [29,30], and whether the phenomenon could influence rates of FFC propagation. Post-corrosion surface analysis of FFC affected surfaces using SEM-EDX is used in combination with the results of in-situ SKP mapping of free corrosion potential distributions to elucidate the mechanism of FFC and explain observations on the influence of chloride ion concentration on propagation rates.

2. Experimental details

2.1. Materials

Three different Mg alloys were used in this study, namely E717 (Electron™ 717), AZ31 and AZ91. The E717 (ZEK100) was supplied in the form of a sheet of 2 mm thickness, provided by Chemetall GmbH with a nominal composition (all weight %): 1.25% Zn, 0.5% Zr, 0.22% Nd, 0.008% Cu, 0.004% Fe, 0.3% others, balance Mg, F temper, cut using electric discharge machining (EDM) into 50 × 50 mm specimens. The AZ31 specimens with a composition (all weight %): 3.1% Al, 0.7% Zn, 0.24% Mn; balance Mg, and the AZ91 specimens with a composition (all weight %): 8.9% Al, 0.8% Zn, and 0.26% Mn with balance Mg were supplied by Magnesium Electron Ltd and cut into 50 mm square coupon by means of electrical discharge machining (EDM). The model coating used in this study is polyvinylbutyral-co-vinyl alcohol-co-vinyl acetate (PVB) with a molecular weight of 70,000–100,000 which was obtained from the Sigma-Aldrich. All other chemicals used in this study have analytical grade purity and were obtained from Sigma-Aldrich.

2.2. Methods

The Mg alloy coupons were subsequently ground using silicon carbide paper up to a 1200 grit surface finish (Buehler CarbiMet™), cleaned with an aqueous detergent solution and rinsed with ethanol. As a height guide, strips of insulating tape were applied on the coupon's edges and a 15.5% w/w ethanolic solution of PVB was applied parallel to the rolling direction of the Mg alloy using the bar casting method. After allowing specimens to dry freely in air, an approximate dry film thickness of 25 μm was determined by means of a micrometre screw gauge. FFC was inoculated by applying controlled quantities of aqueous solutions of either $MgCl_2$, HCl and $FeCl_2$ to a 10 mm long penetrative coating defect, scribed using a fresh scalpel blade perpendicular to the rolling direction of the Mg alloy. In all cases an electrolyte volume of 1 μL was used, injected into the coating defect using a microlitre syringe supplied by Hamilton Ltd.

To understand the effect of the chloride ion concentration on the filiform of coated Mg alloys, four different concentrations of $MgCl_2$ were used: 5×10^{-3} M, 0.02 M, 0.1 M, and 0.5 M. The different levels of relative humidity (RH) 31%, 52%, 76%, 93% and 99% were achieved by using reservoirs containing saturated aqueous solutions of the following: $CaCl_2.2H_2O$, $Ca(NO_3)_2$, NaCl, $Na_2SO_410H_2O$ and DI water at 20 °C [31,32]. After injecting the respective electrolytes into the scribes, the coupons were held in bespoke environmental chambers comprising an optically flat window allowing the coated Mg alloy specimens to be photographed in-situ when maintained in air at a constant RH. Oxygen-free experiments were conducted by holding specimens in similar type of chamber which also comprised an inlet and outlet allowing humidified nitrogen to be introduced in the presence of a saturated salt solution Nitrogen gas was humidified before it was introduced in the container by sparging through three Dreschel bottles connected in series, each containing a saturated solution of $Na_2SO_410H_2O$.

Close-up photographic images of the corroding surface were taken in-situ every 6 h over holding durations of up to 600 h using a Canon EOS 77D camera fitted with AF-microlens and macrotubes. Filiform corrosion affected areas were determined by taking measurements from the photographic images using ImageJ and Photoshop image analysis software. The software was spatially calibrated by setting a number of pixels to an already known distance within the photographic image.

In-situ mapping of free corrosion potential (E_{corr}) distributions associated with PVB-coated E717 specimens undergoing FFC was carried out using Scanning Kelvin Probe (SKP) of in-house construction. Full details of the design and operation of the instrument, along with details of calibration procedure allowing Volta potential differences to be converted to measurements of E_{corr} are given elsewhere [33,34]. The SKP reference probe consisted of a 125 μm diameter gold wire which was vibrated normal to the specimen surface at a vibration frequency of 280 Hz with a 30 μm peak-to-peak amplitude, while the probe-specimen distance was 100 μm. Following initiation of FFC as described above, PVB coated specimens were placed within the environmental chamber of the SKP apparatus and held at a RH of 93%, maintained using reservoirs of the appropriate saturated salt solution. Repetitive scans were carried out every 3 h on a 7 mm × 6 mm area positioned to one side of the scribed defect, using a data point density of 10 points/mm. After calibration the grids of spatially resolved E_{corr} values were visualised as greyscale image maps using the Surfer 10 mapping software. It should be noted that because of the dimensions of the gold wire probe and scan height of 100 μm, the E_{corr} maps will reflect the limited lateral resolution of the SKP instrument, estimated to be of the order of 0.1 mm [35]. On completion of the experiment the PVB coating was carefully peeled

away immediately and the FFC affected region was analysed for Cl^- deposits using a Hitachi TM3000 SEM with integrated Bruker Quantax 70 EDX Analyser.

3. Results and discussion

3.1. Preliminary studies of filiform corrosion

Recently published work demonstrated that in the absence of group I cations, chloride-induced organic coating failure on E717 specimens was characterised by filiform corrosion, consisting of thin, dark tracks which tend to move in a random direction and away from their initiation point [7]. To investigate whether or not the nature of the initiating chloride salt has any effect on the propagation of the FFC on PVB-coated E717, samples were prepared with three penetrative coating scribes into which 1 μL quantities of 0.5 M $FeCl_2$ (left scribe), 1 M HCl (middle scribe) and 0.5 M $MgCl_2$ (right scribe) were injected. The photographic images presented in Fig. 1 show the appearance of the PVB coated E717 Mg alloy at different holding times when held in air at a constant relative humidity of 93% after filiform corrosion initiation. $FeCl_2$ was used to test out a hypothesis of whether enhanced electrocatalytic activity towards cathodic hydrogen evolution (Reaction 1) at the scribe, caused by electrodeposition of metallic iron according to the following displacement reaction,

$$Mg\ (s) + Fe^{2+}\ (aq) \rightarrow Mg^{2+}\ (aq) + Fe\ (s) \quad (3)$$

provides an additional impetus to increase filament propagation rates. In previous work, the corrosion rate of pure Mg immersed in NaCl (aq) can increase by up to a factor of 5 in the presence of dissolved Fe^{2+} (aq) at concentrations of up to 8×10^{-3} M [36].

Upon injection of the different initiating electrolytes, a vigorous reaction involving a rapid darkening of the bare alloy, accompanied by generation of hydrogen bubbles, was observed in all penetrative defects. In the case of $FeCl_2$ (aq), a green colouration was also initially observed which soon turned to brown colour, indicating that aerial oxidation of Fe^{2+}, followed by hydrolysis, occurs in competition to Reaction (3) [36]. Fig. 1b shows that after 1 day exposure to high humidity, several filaments of up to 2 mm in length and varying width have initiated and propagated away from the defect regions in both left and right directions. However, at longer holding times (Fig. 1c and d), neighbouring filaments appear to coalesce, leaving a network of dark corroded surface surrounding the scribes, although individual filament extending up to 10–15 mm away from the scribes can also be identified.

At protracted holding times, the filaments appear to move in a "random walk" manner, where there is no apparent influence of the original rolling direction of the E717 sheet or direction of abrasive cleaning. In addition, from the similarity of the corrosion features observed in the vicinity of each scribed region, it is evident that the nature of the cation has little influence on the morphology or the extent of underfilm corrosion.

The significant visual contrast between uncorroded areas and those affected by filiform-like corrosion was exploited by using image analysis of the time-lapse sequence typified in Fig. 1, as described in Section 2, to generate time-dependent values of FFC area for each scribed region. Typical plots of filiform affected area versus holding time determined for each of the different initiating electrolytes are given in Fig. 2. Average slopes determined over a 200 h holding period, taken from three repeat experiments for each electrolyte type gave FFC area propagation rates of 0.29 ± 0.04, 0.27 ± 0.06 and 0.20 ± 0.03 $mm^2\ h^{-1}$ for $MgCl_2$, $FeCl_2$ and HCl initiating electrolytes respectively. In each case, a linear relationship between corroded area and time required a certain "incubation" time to develop (see Fig. 2), because some of the initial delamination and corrosion product formation in the immediate vicinity of the defect produced general corrosion (uniform darkening) in the 24 h or so after initiation using chloride electrolyte. When $FeCl_2$ was used as the initiating salt, this initial extent of uniform corrosion appeared to be greater than in the case of the other two electrolytes. Therefore, corroded area vs. time slopes quoted above do not include the origin and therefore reflect coating failure rates when only filiform corrosion is propagating.

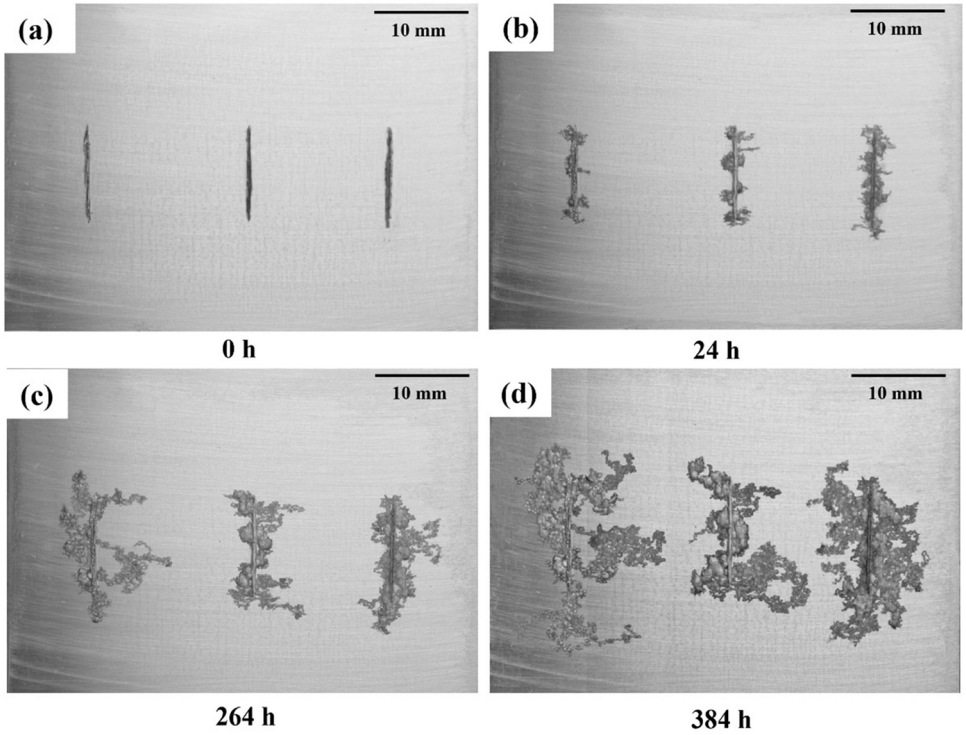

Fig. 1. Photographic images showing the propagation of FFC on a PVB coated E717 alloy specimen held in air at 93% RH and 20 °C following corrosion initiation using controlled quantities of $FeCl_2$ (left scribe), HCl (middle scribe) and $MgCl_2$ (right scribe). Time key: (a) 0 h, (b) 24 h, (c) 264 h and (d) 384 h.

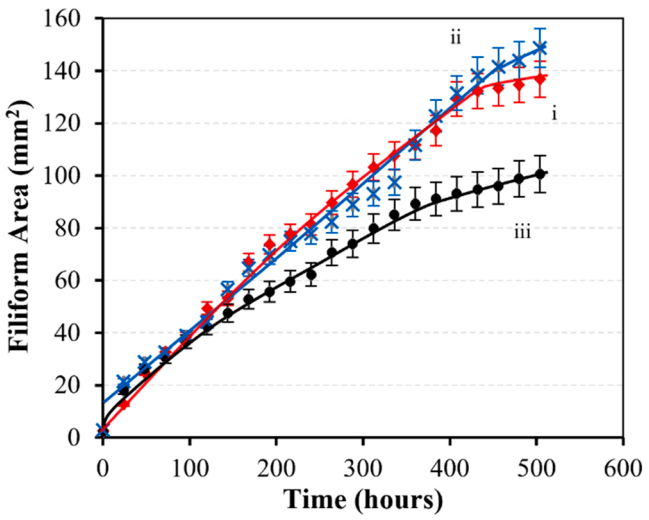

Fig. 2. Plots of FFC area versus time measured for a PVB coated E717 alloy kept in a chamber at 93% RH and 20 °C following initiation of underfilm corrosion using a 1 μL volume of (i) $MgCl_2$, (ii) $FeCl_2$ and (iii) HCl (aq) at a fixed chloride ion concentration of 1 M.

However, in each case, a noticeable deviation from linearity was observed at longer holding times, where area versus time relationships tend to lower gradients. Therefore, although FFC propagation kinetics are similar when divalent chloride salts are used to initiate underfilm corrosion, there is a discernible decrease in rate when HCl is employed. A repeat experiment using a lower chloride ion concentration of 0.2 M, produced the same trend in behaviour, albeit with markedly reduced FFC area propagation rates. The consistently lower rate of underfilm corrosion propagation observed following initiation using HCl is unexpected, given the previously reported rapid development of HCl-induced FFC affecting PVB coated commercially pure Mg [10]. However, as explained in this previous work, the composition of the conserved underfilm electrolyte at the filament leading edges will comprise a concentrated aqueous solution of $MgCl_2$, and a certain induction period will be required in order to generate the requisite composition from HCl (aq) initiated corrosion. If this process is relatively slow, then the known volatility of HCl may mean that less chloride is present than anticipated in order to sustain FFC propagation.

The similarity of the slopes for plots i and ii in Fig. 2 implies that Fe electrodeposition in the defect region has little effect on subsequent FFC propagation, but implies that it may play a role in rapidly generating an appropriate underfilm electrolyte composition to allow FFC to develop in the same manner as when initiated using $MgCl_2$. Following this preliminary investigation of the influence of cation type on chloride-induced FFC, all other systematic studies presented herein were conducted using $MgCl_2$ (aq) as the initiating electrolyte.

In order to determine the distribution of free corrosion potentials over a region of PVB coated E717 affected by actively propagating filaments, the SKP instrument was utilised. Following initiation of FFC by application of a 1 μL volume of 0.5 M of $MgCl_2$ (aq) to a scribed 10 mm long penetrative coating defect, the specimen was subsequently kept in a chamber with high relative humidity of 93% at 21 °C for 10 days to allow filament propagation to take place. Fig. 3(a–e) shows a series of greyscale E_{corr} distribution maps obtained by scanning the surface at regular intervals over a 144-h period. In this particular experiment, an area of 7 mm × 6 mm adjacent to the scribed defect was repetitively scanned using the SKP. The region of interest is indicated by dashed lines in the photographic image given in Fig. 3f, which shows the appearance of the coated surface after the experiment was terminated.

In Fig. 3f three different filaments can be observed, with the main filament of interest denoted as I. This underfilm corrosion feature was the first one to propagate, followed by filaments II and III which develop on the left side of the scan area and generally move towards the right.

The greyscale SKP-derived map (Fig. 3a) indicates that the majority of intact (uncorroded) areas are exhibiting E_{corr} values (E_{intact}) of ca. −1.1 V vs. SHE, but some localised uncorroded regions exhibit potentials which are ± 0.1 V of this mean value. This heterogeneity in E_{intact} values is explained on the basis of atmospheric corrosion occurring in high humidity at the coating/Mg interface producing heterogeneity in the surface (hydro)oxide layer which develops with time. In Fig. 3a–c, changes in E_{corr} distributions as Filament I moves in a diagonal manner, from the centre of the scan area to the top right corner can be observed. The leading edge of the filament appears to adopt more negative potentials than the remainder of the surface, with E_{corr} values ranging between ca. − 1.25 and − 1.35 V vs. SHE. However, as Filament I move from its original location in Fig. 3a, E_{corr} values determined with the region left behind become more positive but remain ca. 100 mV more negative than the surrounding intact surface. Also visible in Fig. 3a and b, is a second filament (denoted II), which initiates in the bottom left corner of the scanned area, elongates by ca. 1 mm and then becomes immobile (i.e. de-activates). Again, the leading edge is characterised by a more negative E_{corr} than the uncorroded surface, although the region becomes less distinct from the surrounding intact surface with time after the filament has ceased to propagate (Fig. 3c–e). In later scans, filament III initiates in the top left corner and moves further inside the scan area, producing a region of more negative local E_{corr} values, which encroaches on the previously corroded tail region of filament I. In Fig. 3d and e it should be noted that the leading edge of filament I has moved beyond the scan area, while its dark corroded tail, extending from the centre of the greyscale map to the top right corner remains slightly depassivated (by ca. 0.1 V) compared to the adjacent uncorroded surface.

After the conclusion of the experiment the sample was withdrawn from the SKP chamber, the PVB coating was carefully peeled away and areas affected by FFC in regions I and III were analysed using SEM/EDX to determine the location of chloride ions. Fig. 4 shows false colour elemental maps superimposed over the secondary electron micrographs of a selection of filiform-like features, where red and green colours correspond with regions of high chloride ion and magnesium abundance respectively. Fig. 4a, along with a higher magnification image in Fig. 4b, show an area of chloride ion activity near the front of a head region.

A similar high abundance of chloride at the leading edge of the filament was also found when a filament was analysed along its entire length as it can be seen from Fig. 4c. These observations using the coated E717 Mg alloy are in agreement with surface analysis findings on commercially pure Mg, where elemental maps obtained using secondary ion mass spectrometry (SIMS) showed chloride ion conservation within the head regions of filament propagating under a PVB coating [10]. However, careful examination of Fig. 4c also shows evidence of chloride ion entrapment within some regions along the length of the filament tail suggesting that not all the chloride ions originally used to initiate FFC are conserved in the leading edges of the filament heads. This observation of Cl^- sequestration within the corrosion product in the tail regions seems consistent with the observation made above that SKP-derived E_{corr} values measured within these regions remain ca. 0.1 V more negative than adjacent uncorroded areas. The distinction between potential values in the head, tail and intact regions of the FFC affected surface may perhaps be more clearly made in Fig. 5, which shows a line profile of E_{corr} versus distance taken along the length of filament I in Fig. 3.

In this particular profile, E_{intact} values of ca. −1.1 V vs. SHE are measured behind the tail region and ahead of the leading edge, while a minimum potential of ca. −1.35 V vs. SHE is observed within the head region. This is similar to typical values of ca. −1.4 V vs. SHE reported previously for FFC leading edges investigated on PVB coated pure Mg under similar conditions [10]. However, the persistence of a low potential of ca. −1.2 V vs. SHE within the tail region is not consistent with previous observation made for pure Mg, where potentials rise to values

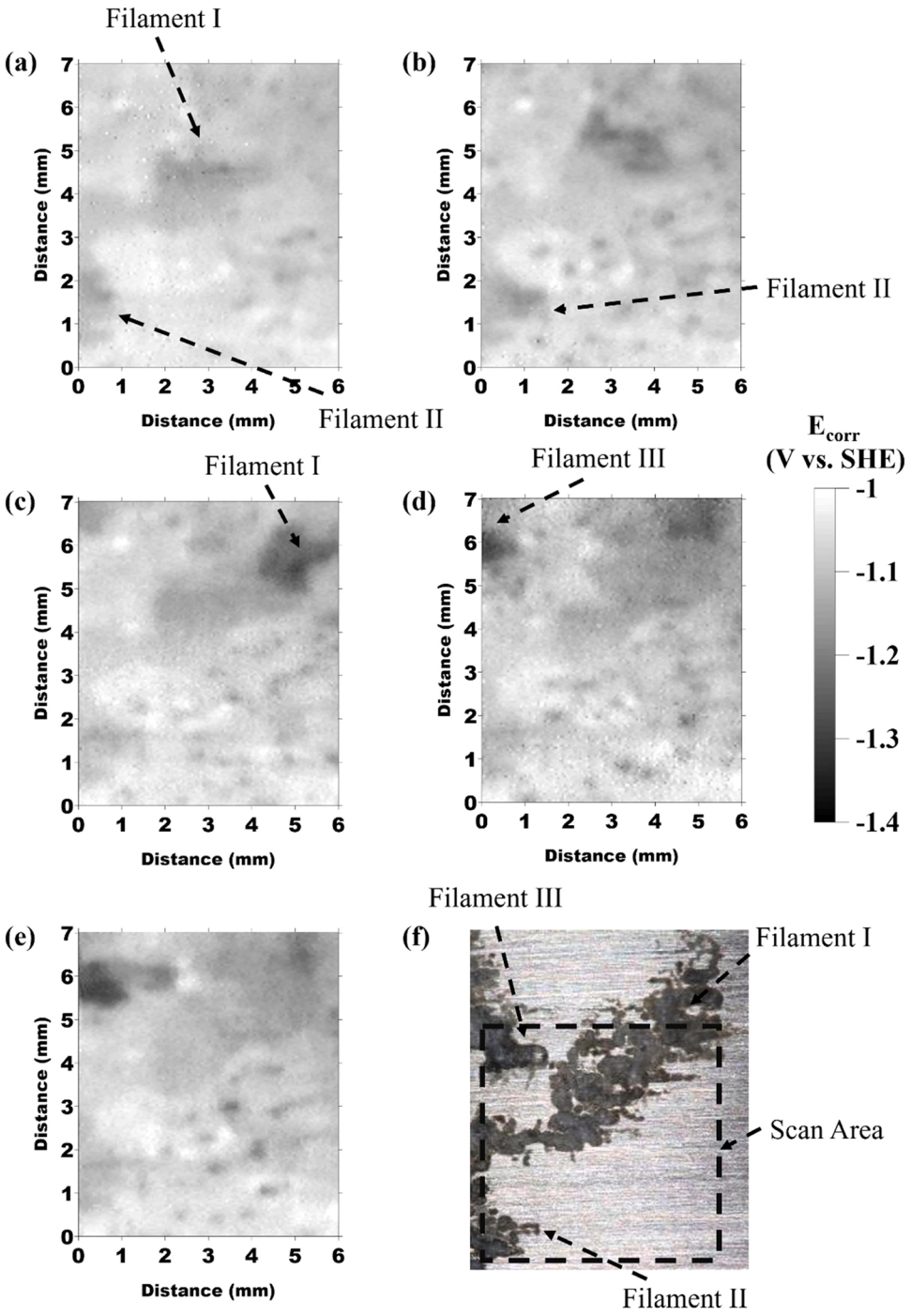

Fig. 3. Greyscale maps showing SKP derived E_{corr} distributions determined at 93% RH and 20 °C for a PVB coated E717 specimen undergoing FFC. Time key: (a) 10 h, (b) 35 h, (c) 60 h, (d) 115 h, (e) 144 h holding times following initiation using a 1 μL quantity of 1 M $MgCl_2$ (aq), while (f) shows a photographic image scan area (indicated by the dashed line) at the end of the experiment.

equal to E_{intact} as filaments move progressively further from their original location. It therefore seems logical to assume that the significantly lower FFC propagation rate on E717, where the elongation of filament I in Fig. 3 proceeds at a rate of ca. 0.04 mm h^{-1} (compared with a rate of 0.1 mm h^{-1} reported for pure Mg), increases the possibility of progressive loss of chloride ions from the head electrolyte via entrapment in the corrosion product filled tail.

3.2. The influence of the chloride ion concentration

It is known that under full immersion conditions, rates of localised corrosion propagation observed on un-coated E717, characterised by the rapid evolution of dark filament-like tracks which lengthen with time and evolve hydrogen at their leading edges, increase significantly with progressively higher sodium chloride concentrations [28]. This current investigation, tests whether or not a similar effect is operational in the development of underfilm filiform corrosion of PVB-coated E717 by varying the concentration of the injected electrolyte and holding the samples in air at a constant 93% relative humidity for 21 days. The effect of applying four different chloride ion concentrations of 1 μL $MgCl_2$ (5×10^{-3}, 0.02, 0.1 and 0.5 M) to a penetrative coating defect on the propagation of FFC was quantified by image analysis of time-lapse image

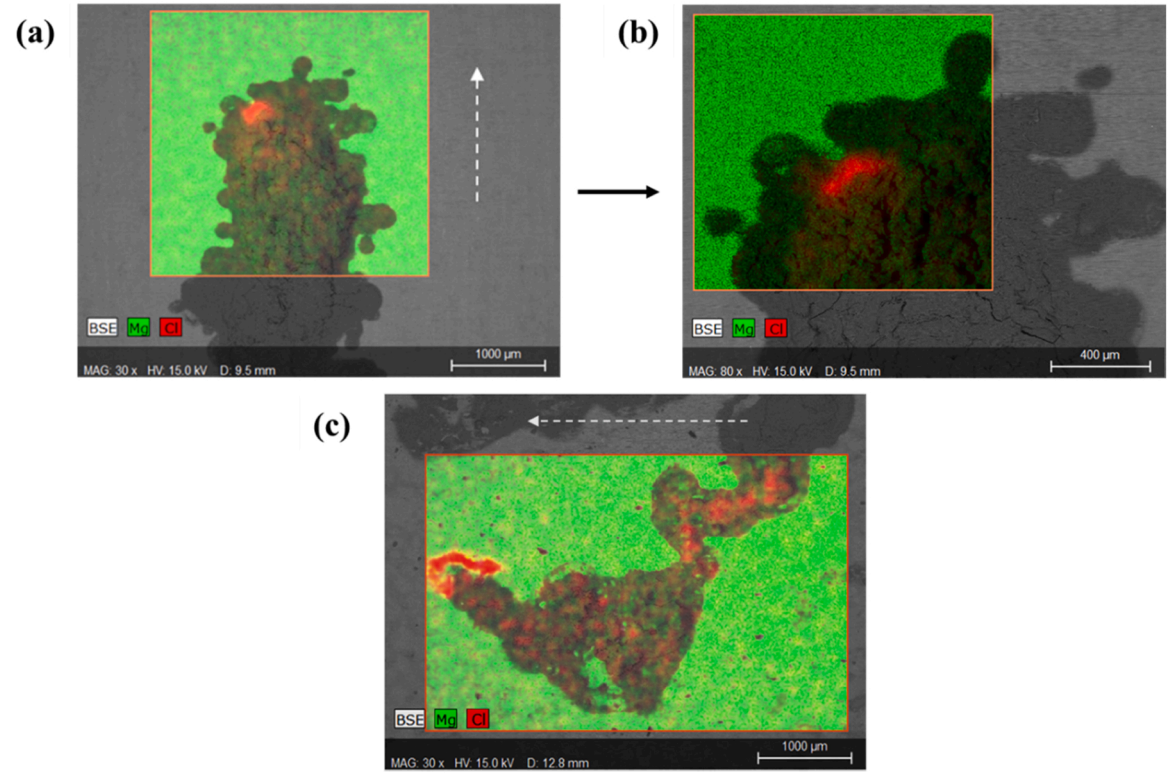

Fig. 4. SEM-EDX images of FFC features on the surface of the E717 Mg alloy after the removal of the PVB coating following corrosion initiation with 1 µL quantity of 1 M $MgCl_2$ (aq). The white arrows indicate the direction of propagation of the filament. (a) shows a typical filament head, along with (b) magnified image of part of this feature, while (c) shows an entire filament consisting of both head and tail regions.

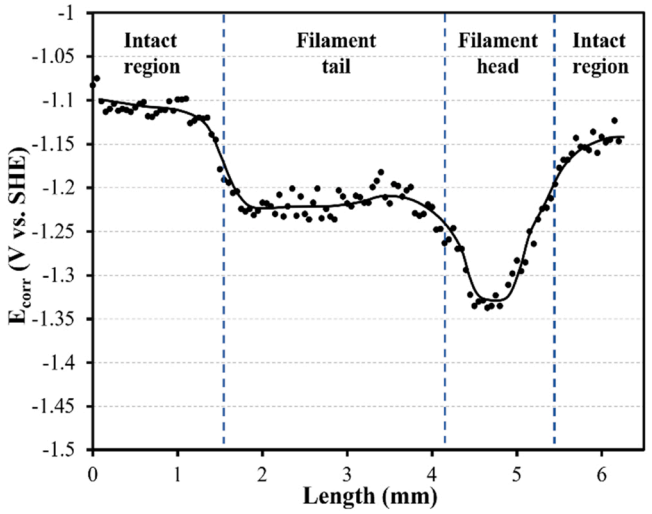

Fig. 5. Plot of E_{corr} values versus distance measured for a propagating filament on a PVB coated E717 specimen exposed to 93% RH and 20 °C.

sequences as discussed previously. Fig. 6 shows the visual appearance of 4 different samples which were scribed and injected with various concentrations of $MgCl_2$ (hereafter abbreviated to $C(MgCl_2)$) and then exposed to 93% relative humidity for 21 days. It is evident that an increase in the concentration of the inoculating electrolyte produces a progressively greater corroded area surrounding the scribes after the same holding time. For specimens which have been inoculated with $C(MgCl_2) \leq 0.02$ M, several discrete filament-like features can be identified, while at higher concentrations the underfilm corrosion morphology suggests that many tracks have coalesced to produce a more uniform disbondment front.

Quantification of the corroded area for the images obtained for each different specimen allowed the effect of chloride ion concentration on the kinetics of underfilm corrosion to be evaluated. Fig. 7 shows typical plots of FFC area versus time for specimens held in air at 93% RH after initiation of corrosion using 1 µL $MgCl_2$ (aq) injections in the concentration range 5×10^{-3} to 0.5 M. The influence of increasing $C(MgCl_2)$ on the extent of the underfilm corroded area associated with each specimen is clearly observed, where final FFC affected areas of 10, 53, 100 and 140 mm^2 were measured for 5×10^{-3}, 0.02, 0.1 and 0.5 M inoculating concentration respectively after a 500-h holding period.

It is also evident that the nature of the FFC area versus time plots is also highly dependent on the quantity of chloride ions used to initiate corrosion. Although an initial linear relationship is observed for each plot in Fig. 7, a significant deviation from linearity is observed at protracted holding times. The time at which the divergence occurs appears to be lengthen with increasing quantity of initiating chloride ion, such that the slope of the area versus time plot tends to zero after 80 h for the lowest $C(MgCl_2)$ used. The point at which an inflection in the linear FFC area versus time relationship is observed, it lengthens progressively with increasing $C(MgCl_2)$ such that a change in the gradient at the highest $MgCl_2$ (aq) initiating concentration occurs after ca. 400 h. At first glance the observations of a deviation from linear FFC area kinetics seems to contradict previous findings obtained using PVB coated commercially pure Mg [10]. However, it should be borne in mind that the aforementioned investigation [10] of pure Mg FFC kinetics was carried out over a significantly shorter timescale and that only a single, high chloride ion concentration was employed.

Initial linear rates of FFC area propagation were also found to depend on the number of moles of chloride ions used to initiate underfilm corrosion. After converting $C(MgCl_2)$ values to the µmol quantity of Cl^- ions applied to the defect (N_{Cl}^-), the initial rate of FFC area propagation (dA/dt) was shown to obey the following empirical relationship:

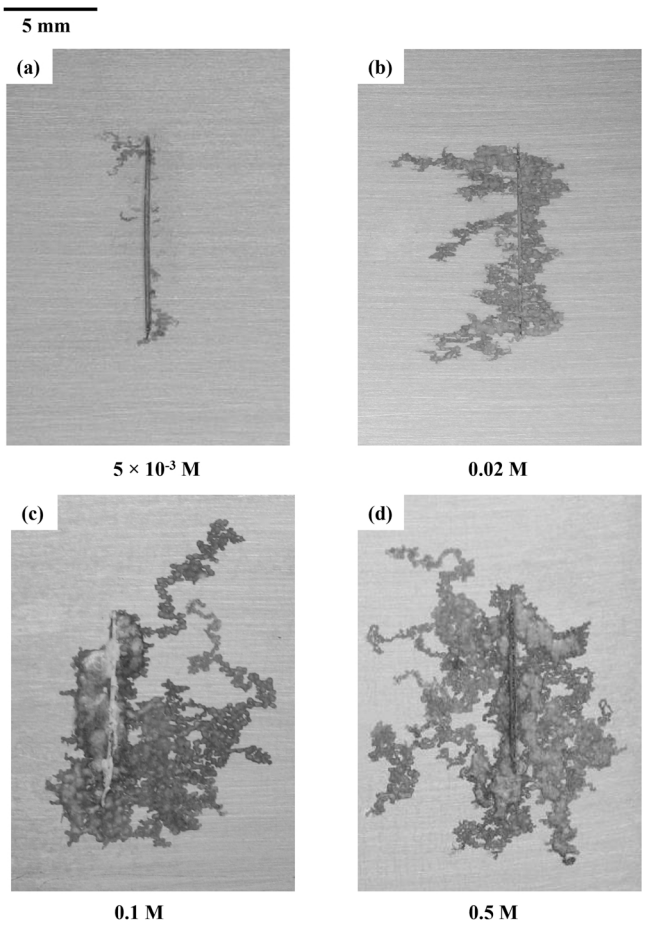

Fig. 6. Photographic images of FFC affecting PVB coated E717 alloy after using $MgCl_2$ concentration of (a) 5×10^{-3}, (b) 0.02, (c) 0.1 and (d) 0.5 M to initiate corrosion and exposing the samples to fixed 93% RH in air for 500 h at 20 °C.

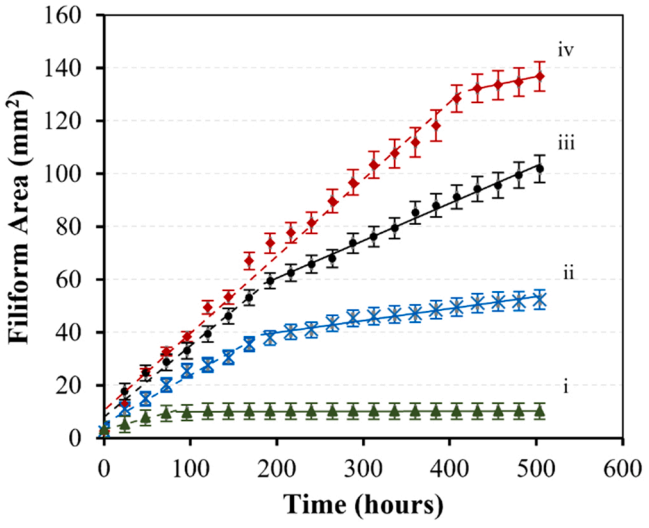

Fig. 7. Plots of FFC area versus time for PVB coated E717 alloy following corrosion initiation using $MgCl_2$ concentrations of (i) 5×10^{-3}, (ii) 0.02, (iii) 0.1, (iv) 0.5 M and subsequent exposure of the coated samples to humid air (93% RH) at 20 °C for 500 h.

$$dA/dt = A + B \log_{10}(N_{Cl}^{-}) \quad (4)$$

with a slope (B) of 0.14 ± 0.02 $mm^2\ h^{-1}$ per decade over a 2 order of magnitude range, and a value of A (equating to the FFC rate measured at 1 μmol applied Cl^- ions) of 0.36 $mm^2\ h^{-1}$. It should be noted that the observed relationship in Eq. (4) was derived from average values of initial dA/dt slopes taken from 3 repeated experiments carried out for each N_{Cl}^-. The logarithmic dependence of dA/dt with N_{Cl}^- differs considerably from predicted relationships derived elsewhere [20] using data derived from a systematic study of the influence of the quantity of hydrochloric acid used to initiate FFC on PVB coated AA2024-T3 alloy specimens. In this particular investigation, dA/dt was predicted to vary as a function $N_{Cl}^{-2/3}$ for a surface-controlled electrochemical process and $N_{Cl}^{-1/3}$ for a system under ohmic control for an equivalent number of individual filaments propagating from a penetrative coating defect to which a controlled quantity of HCl was applied. The lower sensitivity of dA/dt upon N_{Cl}^- observed for E717 Mg surfaces, implied by the logarithmic relationship, suggests that the assumption of complete Cl^- ion conservation within the filament head electrolyte made previously in deriving dA/dt vs. N_{Cl}^- relationships, do not hold true for this alloy. Indeed, the evidence of significant Cl^- ion sequestration within the corrosion product filled tail regions given in Fig. 4, suggests that a substantial fraction of the N_{Cl}^- used to initiate corrosion is removed progressively from the leading edges of the FFC tracks as they propagate, via entrapment within insoluble magnesium hydr(oxide) underfilm deposits or by reaction with the latter to form sparingly soluble magnesium hydroxychloride compounds [37]. The relative insensitivity of dA/dt on N_{Cl}^- observed here, compared to previous FFC kinetic investigations [20], suggests that the rate of Cl^- ion removal from the underfilm head electrolyte increases with N_{Cl}^-, giving rise to the empirically-derived logarithmic dependence given in Eq. (4).

In addition, the deviation from linearity of the FFC area versus time plots shown in Fig. 7 is again consistent with Cl^- ion depletion from the head electrolyte, which will eventually cause filament propagation to cease (at low N_{Cl}^-) or tend to a lower gradient (at higher N_{Cl}^-). The observation that the time at which the inflection in dA/dt gradients occurs increases with N_{Cl}^- also supports the theory that Cl^- ions become progressively lost from the head electrolyte of filament populations. At low N_{Cl}^-, corresponding with the most dilute initiating $C(MgCl_2)$ of 5×10^{-3} M employed, curve i in Fig. 7 may be understood in terms of the corroded area increasing linearly with time as several discrete filaments shown in Fig. 6a (ca. 0.1–0.3 mm width) propagate away from the defect at a mean elongation rate (dL/dt) of 0.05 mm h^{-1} over a holding time of up to 100 h. However, during this time, filaments become visibly narrower and as their widths decrease below 0.1 mm at $t > 100$ h, their forward motion ceases. At the point where all filaments have stopped propagating, then dA/dt (Fig. 7i) becomes zero. The same analysis of individual filaments propagating at a higher initiating $C(MgCl_2)$ of 0.02 M exhibited similar mean velocity values of 0.06 ± 0.01 mm h^{-1}. In addition, filament widths were also seen to decrease by up to 50% over a holding period of 200 h, typically from initial values of ca. 0.5 mm, although for this higher initiating $C(MgCl_2)$, the filaments analysed did not cease to propagate. It can therefore be concluded that varying N_{Cl}^- does not produce significant changes in individual filament velocity and that the increase in dA/dt observed with increasing N_{Cl}^- is principally due to a progressively higher number of individual filaments, which coalesce to form larger unified underfilm corrosion features. The obvious decreases in dA/dt observed at protracted holding times in plots i – iv of Fig. 7 are caused by a progressive removal of Cl^- from the electrolyte filled filament heads, which eventually cause de-activation of individual filaments (curve i) and/or decrease in the filament widths with time.

3.3. The effect of varying relative humidity and the absence of oxygen

Previous studies have shown that the availability and the activity of water at the coating/metal interface is an important controlling factor in the propagation rate of FFC on organic coated pure Mg samples [10]. In the present study, the influence of relative humidity (RH) on FFC corrosion of PVB coated E717 was investigated by varying the relative humidity in the holding environment using saturated salt solutions. The rate of filament propagation was studied using 5 different relative humidity levels of 31%, 53%, 76%, 93% and 99% at a constant temperature of 20 °C. The inoculation of the FFC corrosion was achieved by applying 1 μL of 0.5 M $MgCl_2$ in a penetrative coating defect and the appearance of the samples after 21 days of exposure at varying humidity levels are presented in Fig. 8. From Fig. 8, it is evident that both the lowest and the highest levels of RH did not produce filiform corrosion. The lowest humidity of 31% produced no obvious underfilm corrosion, whereas the highest level of humidity mostly resulted in blistering rather than features which could be identified as FFC (see Fig. 8e). The samples exposed to the intermediate levels of relative humidity in the range 53–93% (see Fig. 8b–d) produced significant FFC in the immediate vicinity of the penetrative defect. The plots of FFC affected area as a function of holding time were determined by analysing the photographic

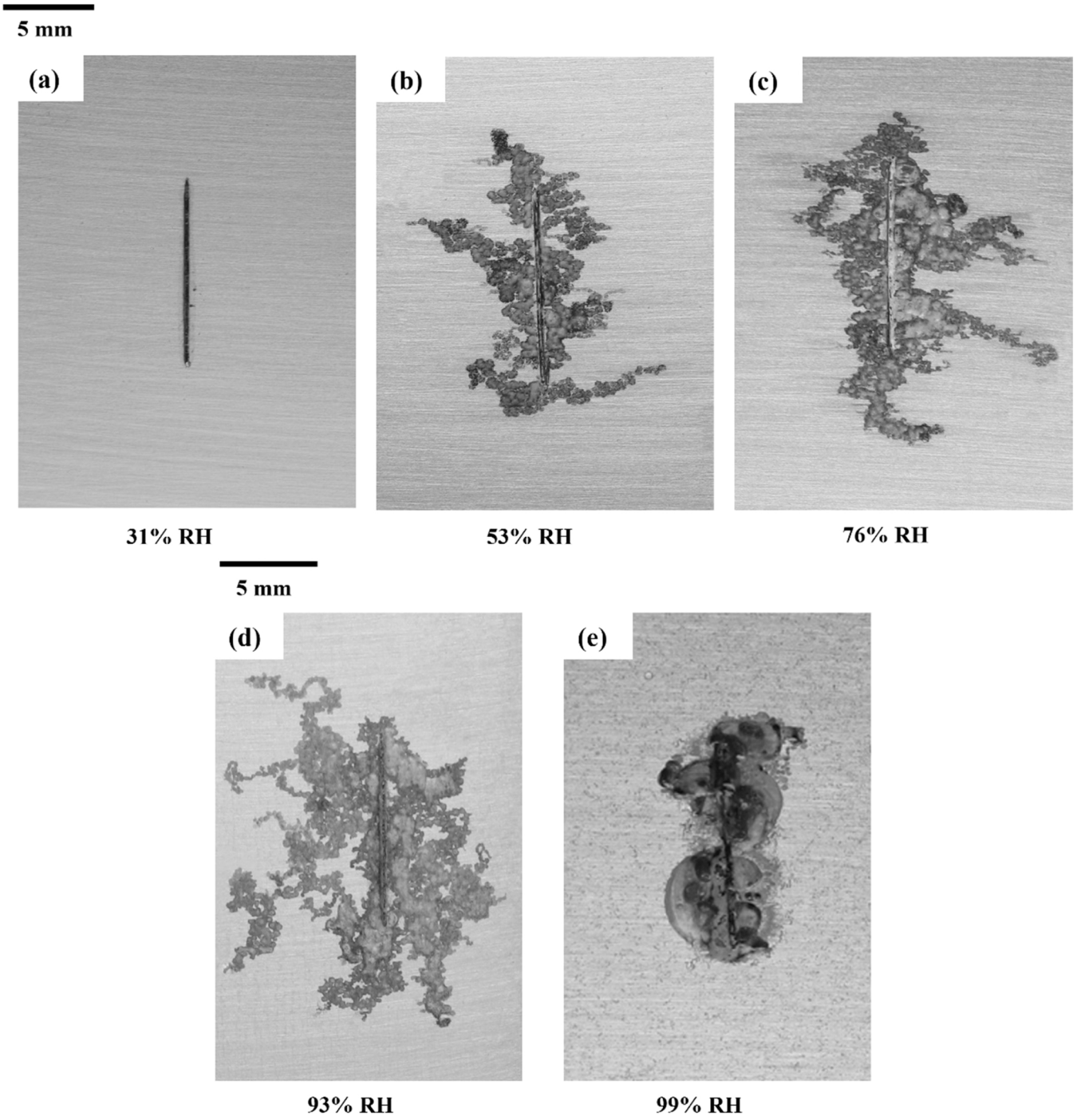

Fig. 8. Photographic images of the appearance of FFC on PVB coated E717 alloy kept in air at 20 °C and a constant RH of (a) 31%, (b) 53%, (c) 76%, (d) 93% and (e) 99% for 500 h following corrosion initiation using 1 μL of 0.5 M $MgCl_2$ (aq).

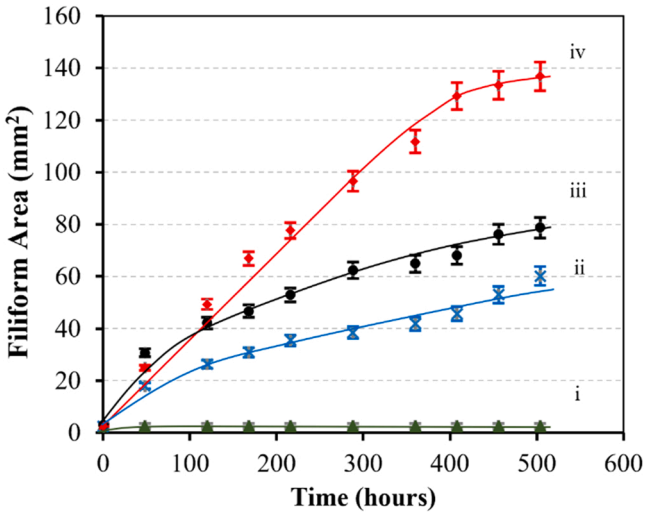

Fig. 9. Plots of FFC area versus time determined for a PVB coated E717 alloy held in air at 20 °C and a fixed RH of (i) 31%, (ii) 53%, (iii) 76% and (iv) 93% following corrosion initiation using 1 μL of 0.5 M $MgCl_2$ (aq).

time-lapse sequences as previously described and are given in Fig. 9.

It has been previously suggested that the main constituent of the electrolyte conserved at the filament head in FFC of organic coated Mg is concentrated $MgCl_2$ (aq) electrolyte [10]. This was borne out of the fact that the reported deliquescence point of $MgCl_2$ is 33% RH [32] and that no Mg FFC was observed when PVB coated pure Mg samples were exposed to relative humidity levels < 31%, [10]. Plot i in Fig. 9 shows that PVB coated E717 behaves in the same manner, again providing supporting evidence that indeed $MgCl_2$ (aq) is the principal constituent of the electrolyte in FFC head regions.

As indicated by the SEM-EDX images in Fig. 4, there is a significant abundance of chloride ions present in the head of the filaments where anodic magnesium dissolution occurs as per Reaction (1). The production of Mg^{2+} (aq) from Reaction (1), along with the conservation of Cl^- supplied by the injected electrolyte, will combine to produce a concentrated aqueous $MgCl_2$ at the anodic leading edge. It would be expected that the highly deliquescent nature of $MgCl_2$ at RH > 31% would cause water to be drawn to the head of the filament via osmosis [10]. However, as relative humidity is increased, it would be expected that the concentration of $MgCl_2$ electrolyte within the filament head would become progressively dilute in order to maintain isopiestic equilibrium with the holding environment. At high RH (>99%), it appears that the head electrolyte composition is unable to support the propagation of filiform-like features and consequently underfilm corrosion takes the form of blistering (Fig. 8e). This transition from FFC to blistering at high RH is consistent with behaviour observed previously on other organic coated metallic substrates to anodic disbondment phenomena [11–13,18]. In the range 31% < RH > 99%, the influence of varying RH is broadly similar to previously reported results obtained over a shorter exposure time for commercially pure Mg in the presence of model PVB coatings [10], where increasing filament propagation rates with RH was directly linked with the availability of water and its transport to the underfilm electrolyte. In this study using E717 Mg substrates a progressive rise in RH from 53% to 93%, (Fig. 9, curves ii–iv) produced an increase in dA/dt from 0.094 to 0.29 $mm^2\ h^{-1}$, measured over the first 400 h of exposure. In terms of final corroded areas after the full 500 h holding time, RH values of 53%, 76% and 93% produced FFC areas of 60, 80 and 140 mm^2 respectively surrounding each penetrative coating defect. An increase in the rate of FFC propagation with RH would be expected, given that the principal underfilm cathodic Reaction is water reduction according to Reaction (1). However, for a fixed N_{Cl}^-, it would also be anticipated that a rise of humidity would also cause the concentration of underfilm $MgCl_2$ (aq) electrolyte within the FFC head regions to become progressively more dilute, in order to maintain isopiestic equilibrium with the holding environment. At first sight, the observation of increasing values of dA/dt with RH seems contradictory with the progressive dilution of $C(MgCl_2)$ at the filament leading edges. However, it should also be noted that for a constant N_{Cl}^-, there would also be a corresponding increase in underfilm electrolyte volume and hence the area of underlying substrate in contact with corrosive electrolyte. As such, providing that the head $C(MgCl_2)$ does not drop below a threshold level required for active propagation, the observation of increased dA/dt with RH can be understood in terms of a progressive increase in underfilm electrolyte area of contact with the E717 substrate.

As discussed previously in Section 3.2, the kinetics of FFC area propagation at 93% RH (Fig. 9 curve iv) show a slight divergence from linearity at protracted holding times. This suggests that the higher rates of propagation may lead to a more rapid exhaustion of the available soluble chlorides from the underfilm electrolyte. This divergence from linearity is not observed for samples subjected to lower levels of relative humidity (Fig. 9 curves ii and iii). The observation seems consistent with the notion of a more concentrated $MgCl_2$ (aq) underfilm electrolyte at lower RH, which in turn would take longer to become depleted of Cl^- ions to reach a threshold concentration at which filament propagation cannot be sustained.

Although water reduction (Reaction 1) is commonly regarded as the predominant cathode reaction on corroding Mg alloy surfaces, recent investigations under both immersion and atmospheric corrosion conditions have demonstrated that oxygen reduction can provide a contribution to the overall cathodic process [38,39]. In order to ascertain the role of oxygen in the FFC of organic coated Mg alloys, a PVB coated E717 sample was placed in a chamber without oxygen (i.e. held in a humidified N_2 flow) and high relative humidity (93%) and underfilm corrosion was initiated as previously using 1 μL of 0.5 M $MgCl_2$ (aq).

The FFC kinetics obtained from this experiment are plotted in Fig. 10 using a corroded area versus time axes and are compared with an experiment carried out in air using the same RH, temperature and initiating $C(MgCl_2)$. The similarity of both plots indicates that the absence of O_2 has little effect on the FFC area propagation rate and in this respect is consistent with observations made previously for filament advance on commercially pure Mg [10].

The insensitivity of filiform advance on E717 substrates to the presence of oxygen confirms the statement that differential aeration

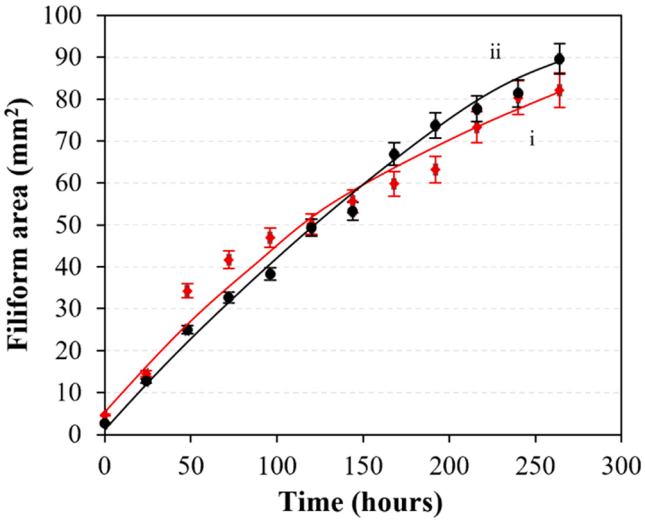

Fig. 10. Plots of FFC area versus time for a PVB coated E717 alloy held at 20 °C and 93% RH in (i) air and (ii) nitrogen following corrosion initiation using 1 μL of 0.5 M $MgCl_2$ (aq).

does not play a role in the underfilm FFC corrosion cell, as is the case for other metals such as iron and aluminium [12,15,18]. Recent work has reported cathodic activation of localised corrosion features, revealed by in-situ scanning vibrating electrode studies of un-coated E717 under immersion in chloride containing aqueous solution [28]. It is therefore proposed the filament advance on E717 substrates involves anodic undermining at the leading edge, driven by cathodic hydrogen evolution on an electro-catalytically enhanced corroded surface at the rear of the electrolyte filled head region. However, given evidence that regions of intense anodic Mg dissolution, according to Reaction (2), are also observed to strongly evolve hydrogen [10], it may be possible that local increases in pressure at the anodic filament leading edges due to hydrogen formation may also play a role by contributing to physical de-adhesion (prying) of the PVB coating from the Mg alloy surface.

3.4. FFC of PVB AZ-series Mg alloys

To further understand the filiform corrosion phenomenon on organic coated Mg alloys, two more Mg alloys were employed in this study, namely the AZ31 and the AZ91 Mg alloy. The presence of aluminium makes these alloys microstructurally different to E717 due to the formation of Al-containing secondary phases and precipitates in the Mg matrix. The presence of principal secondary phases such as $Mg_{17}Al_{12}$ (β-phase) in AZ91 [40,41] and Al–Mn (Al_8Mn_5) intermetallic particles [42] in AZ31 play an important role in the corrosion behaviour of these alloys. However, there is considerable debate on whether the corrosion resistance of Mg increases or decreases with higher aluminium content when un-coated samples are immersed in corrosive aqueous solutions [43–47]. It has been suggested that the relative nobility of the $Mg_{17}Al_{12}$ phase formed in the microstructure of the AZ91 compared to the matrix can enhance the cathodic activity, thus reducing the corrosion resistance of the Mg alloy [48,49]. However, other researchers have stated that this phase can improve the corrosion resistance of Mg by acting as an inert barrier [40,50], thus hindering localised corrosion propagation in the Mg matrix [51]. In a separate study involving bare AZ91 and AZ31 Mg alloys subjected to atmospheric corrosion conditions, the former alloy exhibited superior corrosion resistance [52].

Using the same methodology to initiate underfilm corrosion as with the PVB-coated E717, 1 μL of 0.5 M $MgCl_2$ (aq) was applied to the penetrative scribes and the visual evidence of the filiform corrosion produced on organic coated AZ31 and AZ91 after 2 weeks of exposure to 93% relative humidity and 20 °C are presented in Fig. 11. As in the case of E717, the use of both equivalent quantities of HCl (aq) or $FeCl_2$ (aq) to initiate FFC produced entirely similar results for both AZ alloy types.

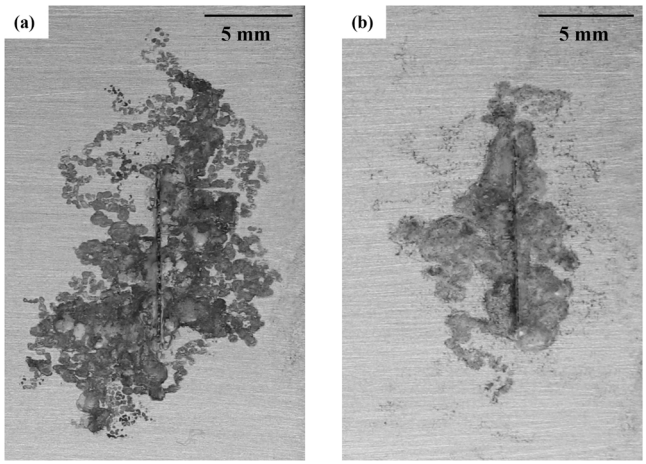

Fig. 11. Photographic images of the appearance of FFC on PVB coated (a) AZ31 and (b) AZ91 samples, 360 h after initiation of corrosion using 1 μL of 0.5 M $MgCl_2$ and holding in air at 93% RH and 20 °C.

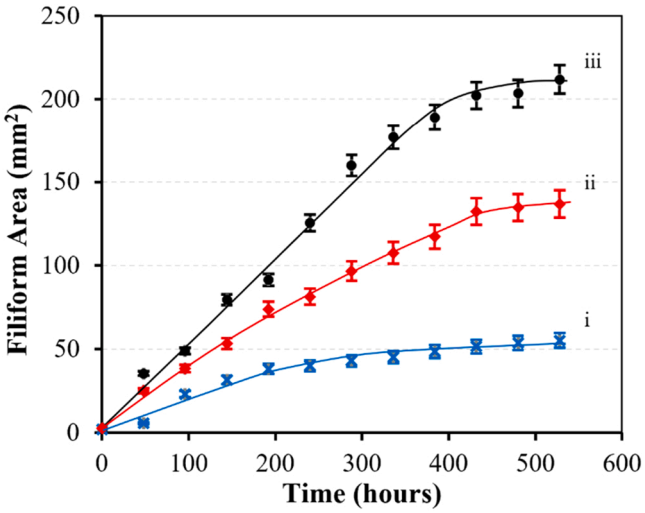

Fig. 12. Plots of FFC area versus time for PVB coated (i) AZ91, (ii) E717 and (iii) AZ31 samples after initiation of underfilm corrosion using 1 μL of 0.5 M $MgCl_2$ and holding in air at 93% RH and 20 °C.

Using the same methodology for time-dependent FFC area quantification as previously, the kinetics of the filiform corrosion rates were analysed for both PVB coated Mg alloys, and these are compared with the area versus time curve for E717 in Fig. 12.

The AZ31B appears to be the most susceptible to FFC, (dA/dt of 0.50 $mm^2\ h^{-1}$ over 400 h), compared to E717 where a dA/dt slope of 0.29 $mm^2\ h^{-1}$ was determined over the same holding time. The AZ91 surface was the most resistant to FFC advance, characterised by a dA/dt value of 0.13 $mm^2\ h^{-1}$ measured under identical conditions. This latter observation seems to support that the presence of a more corrosion resistant $Mg_{17}Al_{12}$ (β-phase) along the grain boundaries, acts as a barrier surrounding the α-matrix [40,53,54], significantly impedes filament advancement when compared to alloys where this phase is absent. Although this does not preclude an influence of aluminium enrichment in the surface oxide of the alpha phase as the alloy Al content is increased also providing enhanced resistance to anodic attack. The higher rate of FFC advance observed for AZ31B in comparison with E717 seems to correlate with previously published observations regarding the propagation of localised corrosion characterised by in-situ SVET analysis under immersion in chloride containing electrolytes [28,55]. In the case of AZ31 immersed in 5% NaCl (aq), local cathodic current density values of ca. − 10 A m^{-2} were measured immediately behind the anodic leading edges of advancing dark corrosion tracks, while under identical conditions, measured values were significantly lower (ca. −5 A m^{-2}). Therefore, the greater extent of cathodic activation of the dark, corroded surface observed for AZ31 may in part account for its higher rate of FFC advance as shown in Fig. 12.

Taking together all the findings discussed herein, a schematic diagram representing the mechanism of atmospheric FFC on organic coated Mg alloys is proposed in Fig. 13. Also shown is the correlation of a typical SKP-derived E_{corr} versus distance profile with the principal features of the underfilm FFC anodic delamination cell. The mechanism is similar to the mechanism of atmospheric FFC on organic coated pure Mg [10], where anodic attack of the alloy surface at the filament leading edge produces a cathodically enhanced corroded surface, which becomes the principal cathode region during filament advance. Although chloride ions are conserved within the head electrolyte due to migration to the anodic leading edge in order to preserve electroneutrality, the findings of this investigation demonstrate that a significant fraction becomes progressively removed via entrapment in the corrosion product-filled filament tail. Consequently, once chloride ion concentration within the head electrolyte decreases below a threshold level capable of sustaining sufficient underfilm corrosion cell current to

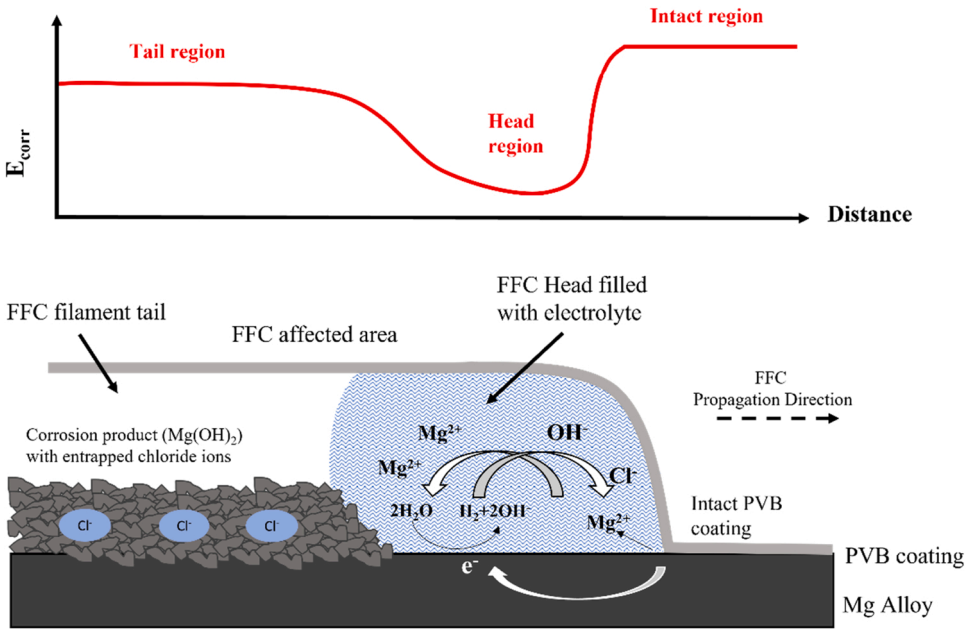

Fig. 13. Schematic diagram of the proposed FFC corrosion mechanism occurring on organic coated Mg alloys with correlation to a typical SKP-derived Ecorr versus distance profile.

maintain filament advance, then the filament will de-activate.

4. Conclusions

- Organic coated Mg alloys are susceptible to filiform corrosion (FFC) as exemplified by the behaviour of PVB coated E717 alloy where underfilm corrosion was initiated by applying different aqueous electrolytes including $MgCl_2$, HCl and $FeCl_2$ to a penetrative coating defect. Once FFC has become established, ensuing FFC propagation rates do not seem to be significantly dependent on the initiating cation.
- The scanning Kelvin Probe (SKP) technique was utilised to map the free corrosion potentials (E_{corr}) associated with regions of PVB-coated E717 surfaces affected by FFC. The leading edge of the filament tracks adopt local E_{corr} values of -1.3 ± 0.05 V vs. SHE, while typical values of -1.1 ± 0.1 V vs. SHE are established over the uncorroded surface. E_{corr} values measured over filament tail regions, left behind the advancing anodic leading edges, are typically 100 mV more negative than the surrounding intact surface.
- FFC propagation rate was shown to be dependent on the number of moles of Cl^- ions (N_{Cl}^-) used to initiate underfilm corrosion. The initial rate of growth of FFC affected areas (dA/dt) was shown to increase as a function of $\log_{10}N_{Cl}^-$. At longer exposure times dA/dt slopes decreased significantly and the time at which an inflection in the A vs. t curve was observed progressively lengthened with increasing N_{Cl}^-. This behaviour is attributed to the progressive depletion of the chloride ions from the filament head electrolyte by entrapment within corrosion product deposits in the tail regions left behind the advancing FFC leading edge. This was confirmed by using SEM-EDX, where chloride ion mapping showed high abundance at individual filament leading edges, but also within areas corresponding to the dark corrosion product filled tails.
- Increasing levels of relative humidity in the range 31–93% in air produced progressively greater rates of FFC propagation, with maximum dA/dt rates measured at 93%. Furthermore, no FFC propagation was observed for samples subjected to 31% RH, corresponding to the deliquescence point of $MgCl_2$, whereas exposure to 99% RH produced a blistering phenomenon. From the aforementioned results, it can be concluded that the water availability in the holding environment plays an important role in the FFC of coated Mg alloys. Additionally, experiments carried out both in the absence and presence of oxygen revealed that the rate of FFC propagation was insensitive to oxygen, since rates of FFC advance were found to be similar in both cases.
- Finally, the FFC behaviour of other technologically important AZ31 and AZ91 series Mg alloys was investigated. Results showed that both PVB coated alloys produced FFC in a similar manner to E717, although propagation rates measured under identical conditions were greater for AZ31, while AZ91 showed the highest resistance to FFC advance.

CRediT authorship contribution statement

Christos Kousis: Methodology, Validation, Formal analysis, Investigation, Data curation, Writing – original draft, Writing – review & editing, Visualization. **Patrick Keil:** Conceptualisation, Methodology, Validation, Supervision. **Neil McMurray:** Conceptualisation, Methodology, Supervision. **Geraint Williams:** Conceptualisation, Formal analysis, Methodology, Validation, Writing – original draft, Writing – review & editing, Supervision.

Declaration of Competing Interest

The authors declare that they have no known competing financial interests or personal relationships that could have appeared to influence the work reported in this paper.

Data Availability

The raw/processed data required to reproduce these findings cannot be shared at this time as the data also forms part of an ongoing study.

Acknowledgements

The support of BASF's Coatings division and Swansea University's EPSRC-funded Centre for Doctoral Training in advanced functional

coatings (COATED[2]), administered through the Materials and Manufacturing Academy, is gratefully acknowledged (EP/L015099/1).

The raw/processed data required to reproduce these findings cannot be shared at this time as the data also forms part of an ongoing study.

References

[1] R.C. Zeng, J. Zhang, W.J. Huang, W. Dietzel, K.U. Kainer, C. Blawert, W. Ke, Review of studies on corrosion of magnesium alloys, Trans. Nonferr. Met. Soc. China Engl. Ed. 16 (2006) 763–771.

[2] M.K. Kulekci, Magnesium and its alloys applications in automotive industry, Int. J. Adv. Manuf. Technol. 39 (2008) 851–865.

[3] J.E. Gray, B. Luan, Protective coatings on magnesium and its alloys – a critical review, J. Alloy. Compd. 336 (2002) 88–113.

[4] X.B. Chen, N. Birbilis, T.B. Abbott, Review of corrosion-resistant conversion coatings for magnesium and its alloys, Corrosion 67 (2011) 35005–35016.

[5] R.G. Hu, S. Zhang, J.-F. Bu, C.-J. Lin, G.L. Song, Progress in organic coatings: recent progress in corrosion protection of magnesium alloys by organic coatings, Prog. Org. Coat. 73 (2011) 129–141.

[6] S. Song, G.L. Song, W. Shen, M. Liu, Corrosion and electrochemical evaluation of coated magnesium alloys, Corrosion 68 (2012) 15005–15012.

[7] G. Williams, C. Kousis, N. McMurray, P. Keil, A mechanistic investigation of corrosion-driven organic coating failure on magnesium and its alloys, npj Mater. Degrad. 3 (2019) 41.

[8] M. van Loo, D.D. Laiderman, R.R. Bruhn, Filiform corrosion, Corrosion 9 (1953) 277–283.

[9] G.M. Hoch, A review of filiform corrosion (filiform corrosion of steel, magnesium and aluminum coated and uncoated surfaces in humid and corrosive atmospheres), in: Proceedings of the International Conference on Localized Corrosion, National Association of Corrosion Engineers, Williamsburg, Va, 1971, p. 1971.

[10] G. Williams, R. Grace, Chloride-induced filiform corrosion of organic-coated magnesium, Electrochim. Acta 56 (2011) 1894–1903.

[11] W. Funke, Blistering of paint films and filiform corrosion, Prog. Org. Coat. 9 (1981) 29–46.

[12] H.N. McMurray, G. Williams, Under film/coating corrosion, in: T.A.J. Richardson (Ed.), Corrosion in Liquids, Types of Corrosion in Liquids, Shreir's Corrosion, Vol. 2, 4th ed., Elsevier, 2009, p. 988.

[13] B. Liu, Y. Wei, W. Chen, L. Hou, C. Guo, Blistering failure analysis of organic coatings on AZ91D Mg-alloy components, Eng. Fail. Anal. 42 (2014) 231–239.

[14] C.F. Sharman, Filiform underfilm corrosion of lacquered steel surfaces, Nature 153 (1944) 621–622.

[15] R.T. Ruggeri, T.R. Beck, An analysis of mass transfer in filiform corrosion, Corrosion 39 (1983) 452–465.

[16] C. Hahin, Localised corrosion, in: S.C. Dexter (Ed.), Metals Handbook, 9th ed. Vol. 13, American Society for Metals, Metals Park, OH, 1987, pp. 104–122.

[17] G. Williams, H.N. McMurray, The mechanism of group (I) chloride initiated filiform corrosion on iron, Electrochem. Commun. 5 (2003) 871–877.

[18] A. Bautista, Filiform corrosion in polymer-coated metals, Prog. Org. Coat. 28 (1996) 49–58.

[19] W. Schmidt, M. Stratmann, Scanning kelvinprobe investigations of filiform corrosion on aluminum alloy 2024-t3, Corros. Sci. 40 (1998) 1441–1443.

[20] G. Williams, H.N. McMurray, The kinetics of chloride-induced filiform corrosion on aluminum alloy AA2024-T3, J. Electrochem. Soc. 150 (2003) B380–B388.

[21] T.M. Watson, A.J. Coleman, G. Williams, H.N. McMurray, The effect of oxygen partial pressure on the filiform corrosion of organic coated iron, Corros. Sci. 89 (2014) 46–58.

[22] M.P. Brady, W.J. Joost, C.D. Warren, Insights from a recent meeting: current status and future directions in magnesium corrosion research, Corrosion 73 (2017) 452–462.

[23] X.P. Niu, T. Skszek, M. Fabischek, A. Zak, Low temperature warm forming of magnesium ZEK 100 sheets for automotive applications, Mater. Sci. Forum 783–786 (2014) 431–436.

[24] R.M. Asmussen, W.J. Binns, P. Jakupi, D. Shoesmith, The influence of microstructure on the corrosion of magnesium alloy ZEK100, Corrosion 71 (2014) 242–254.

[25] M.P. Brady, G. Rother, L.M. Anovitz, K.C. Littrell, K.A. Unocic, H.H. Elsentriecy, G.-L. Song, J.K. Thomson, N.C. Gallego, B. Davis, Film breakdown and nano-porous $Mg(OH)_2$ formation from corrosion of magnesium alloys in salt solutions, J. Electrochem. Soc. 162 (2015) C140–C149.

[26] M.P. Brady, D.N. Leonard, H.M. Meyer, J.K. Thomson, K.A. Unocic, H. H. Elsentriecy, G.-L. Song, K. Kitchen, B. Davis, Advanced characterization study of commercial conversion and electrocoating structures on magnesium alloys AZ31B and ZE10A, Surf. Coat. Technol. 294 (2016) 164–176.

[27] B. Zaghloul, J.R. Kish, Corrosion inhibition of Mg alloy ZEK100 sheet metal by dissolved lithium carbonate, J. Electrochem. Soc. 168 (2021) 81507.

[28] C. Kousis, N. McMurray, P. Keil, G. Williams, The influence of chloride ion concentration on the localized corrosion of E717 magnesium alloy, Corrosion 77 (2020) 156–167.

[29] S.V. Lamaka, D. Höche, R.P. Petrauskas, C. Blawert, M.L. Zheludkevich, A new concept for corrosion inhibition of magnesium: suppression of iron re-deposition, Electrochem. Commun. 62 (2016) 5–8.

[30] D. Mercier, J. Światowska, S. Zanna, A. Seyeux, P. Marcus, Role of segregated iron at grain boundaries on Mg corrosion, J. Electrochem. Soc. 165 (2018) C42–C49.

[31] L. Greenspan, Humidity fixed points of binary saturated aqueous solutions, Res. Natl. Inst. Stand. Technol. 81 (1977) 89–96.

[32] R.C. Weast, CRC Handbook of Chemistry and Physics, J. Chem. Technol. Biotechnol., CRC Press, Boca Raton, FL, 1987.

[33] G. Williams, H.N. McMurray, Chromate inhibition of corrosion-driven organic coating delamination studied using a scanning kelvin probe technique, J. Electrochem. Soc. 148 (2001) B377–B385.

[34] G. Williams, H.N. McMurray, D.A. Worsley, Latent fingerprint detection using a scanning Kelvin microprobe. J. Forensic Sci. (2001).

[35] H.N. McMurray, G. Williams, Probe diameter and probe–specimen distance dependence in the lateral resolution of a scanning Kelvin probe, J. Appl. Phys. 91 (2002) 1673–1679.

[36] E. Michailidou, H.N. McMurray, G. Williams, Quantifying the role of transition metal electrodeposition in the cathodic activation of corroding magnesium, J. Electrochem. Soc. 165 (2018) C195–C205.

[37] C. Mažuranić, H. Bilinski, B. Matković, Reaction products in the system $MgCl_2$-NaOH-H_2O, J. Am. Ceram. Soc. 65 (1982) 523–526.

[38] E.L. Silva, S.V. Lamaka, D. Mei, M.L. Zheludkevich, The reduction of dissolved oxygen during magnesium corrosion, ChemistryOpen 7 (2018) 664–668.

[39] M. Strebl, S. Virtanen, Real-time monitoring of atmospheric magnesium alloy corrosion, J. Electrochem. Soc. 166 (2019) C3001–C3009.

[40] O. Lunder, J.E. Lein, T.K. Aune, K. Nisancioglu, The role of Mg17Al12 phase in the corrosion of Mg alloy AZ91, Corrosion 45 (1989) 741–748.

[41] M. Jönsson, D. Thierry, N. LeBozec, The influence of microstructure on the corrosion behaviour of AZ91D studied by scanning Kelvin probe force microscopy and scanning Kelvin probe, Corros. Sci. 48 (2006) 1193–1208.

[42] G. Hamu, D. Eliezer, L. Wagner, The relation between severe plastic deformation microstructure and corrosion behavior of AZ31 magnesium alloy, J. Alloy. Compd. 468 (2009) 222–229.

[43] A. Pardo, M.C. Merino, A.E. Coy, R. Arrabal, F. Viejo, E. Matykina, Corrosion behaviour of magnesium/aluminium alloys in 3.5wt% NaCl, Corros. Sci. 50 (2008) 823–834.

[44] L. Wang, T. Shinohara, Z.B.P. Zhang, Corrosion behavior of Mg, AZ31, and AZ91 alloys in dilute NaCl solutions, J. Solid State Chem. 14 (2010) 1897–1907.

[45] M.C. Zhao, P. Schmutz, S. Brunner, M. Liu, G. Song, A. Atrens, An exploratory study of the corrosion of Mg alloys during interrupted salt spray testing, Corros. Sci. 51 (2009) 1277–1292.

[46] G. Song, A. Atrens, M. Dargusch, Influence of microstructure on the corrosion of diecast AZ91D, Corros. Sci. 41 (1999) 249–273.

[47] B. Genevieve, C. Blanc, N. Pébère, AC impedance spectroscopy in characterizing time-dependent corrosion of AZ91 and AM50 magnesium alloys characterization with respect to their microstructures, J. Electrochem. Soc. 148 (2001) B489–B496.

[48] K. Gusieva, C.H.J. Davies, J.R. Scully, N. Birbilis, Corrosion of magnesium alloys: the role of alloying, Int. Mater. Rev. 60 (2014) 169–194.

[49] G.L. Song, Recent progress in corrosion and protection of magnesium alloys, Adv. Eng. Mater. 7 (2005) 563–586.

[50] F.H. Froes, Y.W. Kim, F. Hehmann, Rapid solidification of Al, Mg and Ti, JOM 39 (1987) 14–21.

[51] M.C. Zhao, P.J. Uggowitzer, M. Liu, P. Schmutz, G. Song, A. Atrens, Corrosion of AZ91 – influence of the β-phase morphology, in: M.S. Dargusch, S. Keay (Eds.), Materials Science Forum, Vol. 618–619, Light Metals Technology, 2009, pp. 473–478.

[52] M. Esmaily, D.B. Blücher, J.E. Svensson, M. Halvarsson, L.G. Johansson, New insights into the corrosion of magnesium alloys – the role of aluminum, Scr. Mater. 115 (2016) 91–95.

[53] M.C. Zhao, M. Liu, G. Song, A. Atrens, Influence of the β-phase morphology on the corrosion of the Mg alloy AZ91, Corros. Sci. 50 (2008) 1939–1953.

[54] G.L. Song, A. Atrens, Corrosion mechanisms of magnesium alloys, Adv. Eng. Mater. 1 (1999) 11–33.

[55] G. Williams, H. ap Llwyd Dafydd, R. Grace, The localised corrosion of Mg alloy AZ31 in chloride containing electrolyte studied by a scanning vibrating electrode technique, Electrochim. Acta 109 (2013) 489–501.